A&A 488, 653–666 (2008)
DOI: 10.1051/0004-6361:200810031

Astronomy & Astrophysics

The Alpha Centauri binary system⋆,⋆⋆

Atmospheric parameters and element abundances

G. F. Porto de Mello, W. Lyra⋆⋆⋆, and G. R. Keller†

Universidade Federal do Rio de Janeiro, Observatório do Valongo, Ladeira do Pedro Antônio, 43, CEP: 20080-090, Rio de Janeiro, RJ, Brazil
e-mail: gustavo@ov.ufrj.br

Received 23 April 2008 / Accepted 20 June 2008

ABSTRACT

Context. The α Centauri binary system, owing to its duplicity, proximity and brightness, and its components' likeness to the Sun, is a fundamental calibrating object for the theory of stellar structure and evolution and the determination of stellar atmospheric parameters. This role, however, is hindered by a considerable disagreement in the published analyses of its atmospheric parameters and abundances.

Aims. We report a new spectroscopic analysis of both components of the α Centauri system, compare published analyses of the system, and attempt to quantify the discrepancies still extant in the determinations of the atmospheric parameters and abundances of these stars.

Methods. The analysis is differential with respect to the Sun, based on spectra with $R = 35\,000$ and signal-to-noise ratio $\geq$1000, and employed spectroscopic and photometric methods to obtain as many independent $T_{\rm eff}$ determinations as possible. We also check the atmospheric parameters for consistency against the results of the dynamical analysis and the positions of the components in a theoretical HR diagram.

Results. The spectroscopic atmospheric parameters of the system are found to be $T_{\rm eff} = (5847 \pm 27)$ K, [Fe/H] $= +0.24 \pm 0.03$, $\log g = 4.34 \pm 0.12$, and $\xi_t = 1.46 \pm 0.03$ km s^{-1}, for α Cen A, and $T_{\rm eff} = (5316 \pm 28)$ K, [Fe/H] $= +0.25 \pm 0.04$, $\log g = 4.44 \pm 0.15$, and $\xi_t = 1.28 \pm 0.15$ km s^{-1} for α Cen B. The parameters were derived from the simultaneous excitation & ionization equilibria of Fe I and Fe II lines. $T_{\rm eff}$s were also obtained by fitting theoretical profiles to the Hα line and from photometric calibrations.

Conclusions. We reached good agreement between the three criteria for α Cen A. For α Cen B the spectroscopic $T_{\rm eff}$ is ~140 K higher than the other two determinations. We discuss possible origins of this inconsistency, concluding that the presence of non-local thermodynamic equilibrium effects is a probable candidate, but we note that there is as yet no consensus on the existence and cause of an offset between the spectroscopic and photometric $T_{\rm eff}$ scales of cool dwarfs. The spectroscopic surface gravities also agree with those derived from directly measured masses and radii. An average of three independent $T_{\rm eff}$ criteria leads to $T_{\rm eff}$ (A) $= (5824 \pm 26)$ K and $T_{\rm eff}$ (B) $= (5223 \pm 62)$ K. The abundances of Na, Mg, Si, Mn, Co, and Ni and, possibly, Cu are significantly enriched in the system, which also seems to be deficient in Y and Ba. This abundance pattern can be deemed normal in the context of recent data on metal-rich stars. The position of α Cen A in an up-to-date theoretical evolutionary diagram yields a good match of the evolutionary mass and age (in the 4.5 to 5.3 Gyr range) with those from the dynamical solution and seismology, but only marginal agreement for α Cen B, taking into account its more uncertain $T_{\rm eff}$.

Key words. stars: abundances – stars: fundamental parameters – stars: late-type – techniques: spectroscopic – stars: individual: α Centauri

1. Introduction

The α Centauri binary system, composed of two solar-type stars (HD 128620 and 128621), is one of the brightest in the sky and figures as our second closest galactic neighbor, 1.34 parsec away. The star closest to the Sun is the M5.5 dwarf Proxima Centauri (Gliese & Jahreiss 1991), ~15 000 AU away from the α Centauri binary, and its gravitational connection to the system is still a topic of controversy. Anosova et al. (1994) proposed that Proxima has a hyperbolic orbit around the inner pair, and that the three stars might form part of a more extended kinematical group. Wertheimer & Laughlin (2006), however, found the distance between Proxima and the pair to be comparable to the Hill radius of the latter, whereby the Galactic potential becomes dominant over that of the inner pair and the system becomes unbound. These authors favor the existence of a physically-bound triple system, suggesting that Proxima is presently at the apoastron of its orbit. Highly precise monitoring of radial velocity variations of the system by Endl et al. (2001) constrains the upper limit of the mass of putative planetary or substellar companions of the system at less than 3.5 Jupiter masses (actually less than one Saturn mass if coplanar orbits are assumed).

The proximity of the α Centauri system provides a well-determined parallax, and its brightness allows for the acquisition of extremely high-quality spectra. Moreover, its binary nature and relatively short period of 80 years enables the

⋆ Based on observations collected at Observatório do Pico dos Dias (OPD), operated by the Laboratório Nacional de Astrofísica, CNPq, Brazil.

⋆⋆ Table 2 is only available in electronic form at http://www.aanda.org

⋆⋆⋆ *Present address*: Department of Physics and Astronomy, Uppsala Astronomical Observatory, Box 515, 751 20 Uppsala, Sweden.

† *Present address*: Universidade de São Paulo, Instituto de Astronomia, Geofísica e Ciências Atmosféricas, Depto. de Astronomia, Rua do Matão 1226, CEP: 05508-900, São Paulo, SP, Brazil.

Table 1. Literature determinations of atmospheric parameters for α Cen A and B.

α **Centauri A**						
Reference	Atmospheric parameter				Method used	
	$T_{\rm eff}$ (K)	$\log g$	ξ_t (km s^{-1})	[Fe/H]	$T_{\rm eff}$	$\log g$
French & Powell (1971)	5770	–	–	+0.22	*a*	–
Soderblom (1986)	5770	–	–	–	*b*	–
England (1980)	5750	4.38	1.0	+0.28	*b, c, d*	*c, d*
Bessell (1981)	5820	4.25	1.7	−0.01	*a, e*	*e*
Smith et al. (1986)	5820	4.40	1.54	+0.20	*a, e*	*d*
Gratton & Sneden (1987)	5750	4.38	1.2	+0.11	*f*	*c, e*
Abia et al. (1988)	5770	4.5	1.0	+0.22	*b*	*f*
Edvardsson (1988)	–	4.42	–	+0.28	–	*d*
Furenlid & Meylan (1990)	5710	4.27	1.0	+0.12	*a, e*	*e*
Chmielewski et al. (1992)	5800	4.31	–	+0.22	*b*	*c*
Neuforge-Verheecke & Magain (1997)	5830	4.34	1.09	+0.25	*a*	*ce*
Allende-Prieto et al. (2004)	5519	4.26	1.04	+0.12	*f*	*c*
Doyle et al. (2005)	5784	4.28	1.08	+0.12	*direct*	*direct*
Santos et al. (2005)	5844	4.30	1.18	+0.28	*a*	*a*
del Peloso et al. (2005a)	5813	4.30	1.23	+0.26	*b, f*	*c*
Valenti & Fischer (2005)	5802	4.33	–	+0.23	*a*	*e*
This work	5824	4.34	1.46	+0.24	*a, b, e, f*	*c, e*
α **Centauri B**						
Reference	Atmospheric parameter				Method used	
	$T_{\rm eff}$ (K)	$\log g$	ξ_t (km s^{-1})	[Fe/H]	$T_{\rm eff}$	$\log g$
French & Powell (1971)	5340	–	–	+0.12	*a*	–
Soderblom (1986)	5350	–	–	–	*b*	–
England (1980)	5260	4.73	1.1	+0.38	*b, c, e*	*c, e*
Bessell (1981)	5350	4.5	1.0	−0.05	*a, e*	*e*
Smith et al. (1986)	5280	4.65	1.35	+0.20	*a, e*	*d*
Gratton & Sneden (1987)	5250	4.50	1.0	+0.08	*f*	*c, e*
Abia et al. (1988)	5300	4.5	1.5	+0.14	*b*	*f*
Edvardsson (1988)	–	4.65	–	+0.32	–	*d*
Chmielewski et al. (1992)	5325	4.58	–	+0.26	*b*	*c*
Neuforge-Verheecke & Magain (1997)	5255	4.51	1.00	+0.24	*a*	*c, e*
Allende-Prieto et al. (2004)	4970	4.59	0.81	+0.18	*f*	*c*
Santos et al. (2005)	5199	4.37	1.05	+0.19	*a*	*a*
Valenti & Fischer (2005)	5178	4.56	–	+0.22	*a*	*e*
This work	5223	4.44	1.28	+0.25	*a, b, e, f*	*c, e*

The notation used from Cols. 6 to 7 stands for: *a* excitation equilibrium; *b* wings of Balmer lines; *c* trigonometric parallax; *d* wings of strong lines; *e* ionization equilibrium; *f* photometric color indexes; *direct* directly-measured luminosity, mass and radius. Note that, generally, the microturbulence velocities have not the same zero point and cannot be directly compared. Typical errors, respectively, in $T_{\rm eff}$, $\log g$, and [Fe/H] are ≤100 K, ≤0.2 dex, and ≤0.1 dex, but note that these estimates usually do not include systematic uncertainties, and that not all authors provide error determinations, or labor under the same definitions for them.

hypothesis-free accurate determination of masses (Pourbaix et al. 1999, 2002). If we couple to these facts their being very solar-like, the α Centauri stars thus appear as objects of fundamental importance in the calibration of evolutionary tracks, theoretical isochrones, and model atmospheres, hence the great interest in the precise determination of their atmospheric parameters, evolutionary state, and chemical composition.

The brightness of the system's components also favor the determination of internal structure and state of evolution by seismological observations. The analysis of the frequency spectrum and amplitudes of both photometric and spectroscopic oscillations in the outer layers of solar-type stars, driven by convection, can yield otherwise unobtainable information on internal structure, such as the depth of the convection zone and the density and temperature profiles. They can also provide independent checks on stellar masses, ages, and chemical composition. Yildiz (2007), Eggenberger et al. (2004), and Thoul et al. (2003) have agreed on an age for the system between 5.6 and 6.5 Gyr. Miglio & Montalbán (2005) propose model-dependent ages in the 5.2 to 7.1 Gyr interval. However, they also note that fixing the non-seismic observables, namely masses and radii, leads to an age as large as 8.9 Gyr, proposing that further seismological observations may be needed to clarify this apparent discrepancy between the independent observation of the oscillation spectra and the directly-measured masses and radii. The previous analysis of Guenther & Demarque (2000) favors a slightly higher age of ∼7.6 Gyr. The masses are very well constrained at $M_{\rm A} = 1.105 \pm 0.007$ and $M_{\rm B} = 0.934 \pm 0.006$ in solar masses (Pourbaix et al. 2002), which, along with interferometrically measured (in solar units) radii of $R_{\rm A} = 1.224 \pm 0.003$ and $R_{\rm B} = 0.863 \pm 0.005$ (Kervella et al. 2003) yield surface gravities (in c.g.s. units) of $\log g_{\rm A} = 4.307 \pm 0.005$ and $\log g_{\rm B} = 4.538 \pm 0.008$, an accuracy seldom enjoyed by stellar spectroscopists. Altogether these data pose very tight constrains on the modelling of fundamental quantities of internal structure, such as mixing-length parameters and convection zone depths.

Nevertheless, the state of our current understanding of this system still lags behind its importance, since published spectroscopic analyses reveal considerable disagreement in the determination of atmospheric parameters and chemical abundances, particularly for component B, though most authors agree that

the system is significantly metal-rich with respect to the Sun. A non-exhaustive review is given in Table 1. This fact is embarrassing, even in our modern era of massive surveys, since the individual study of key objects is necessary to quantify systematic errors that might be lurking inside huge databases and cannot be reduced with large number statistics. Indeed, considering only those analyses since the 90 s, eight performed a detailed analysis of the atmospheric parameters and chemical composition of α Cen A: Furenlid & Meylan (1990), hereafter FM90; Chmielewski et al. (1992), Neuforge-Verheecke & Magain (1997), Allende-Prieto et al (2004), hereafter ABLC04; del Peloso et al. (2005a), Santos et al. (2005), Valenti & Fisher (2005), and Doyle et al. (2005). Five of them also performed this analysis for the cooler and fainter component α Cen B: Chmielewski et al. (1992), Neuforge-Verheecke & Magain (1997), ABLC04; Valenti & Fisher (2005) and Santos et al. (2005). All these authors, but Chmielewski et al. (1992) and Santos et al. (2005), obtained abundances for many chemical elements other than iron.

The analysis of FM90 for α Cen A is noteworthy in that it was the first to imply an abundance pattern considerably different from solar, with excesses relative to Fe in Na, V, Mn, Co, Cu, and deficits in Zn and the heavy neutron capture elements. The authors also proposed a low $T_{\rm eff}$ and a near solar metallicity for component A, in contrast with most previously published figures. These authors invoked a supernova to explain the peculiar chemical features of the system. The next analysis (Chmielewski et al. 1992) sustained a high $T_{\rm eff}$ and appreciably higher metallicity for the system, which was also obtained by Neuforge-Verheecke & Magain (1997). The latter authors, moreover, found an abundance pattern not diverging significantly from that of the Sun, though supporting the deficiency of heavy elements found by FM90.

The papers of del Peloso et al. (2005a) and Santos et al. (2005) both derived a high metallicity for the system. Doyle et al. (2005) added to the controversy by proposing both a low $T_{\rm eff}$ and a metallicity not appreciably above solar for component A, as did FM90. Their abundance pattern is, however, solar. ABLC04 propose for both components much lower $T_{\rm eff}$s than previously found by any author. Even though their metallicity agrees reasonably with that of Chmielewski et al. (1992) and Neuforge-Verheecke & Magain (1997), their detailed abundance pattern is highly non-solar and also very different from any thus far, with high excesses of Mg, Si, Ca, Sc, Ti, Zn and Y. Their low metallicity is a result of a lower adopted $T_{\rm eff}$, as also is the case for the FM90 analysis.

Doyle et al. (2005) presented the most recent abundance analysis of α Cen A and obtained abundances for six elements. They made use of the Anstee, Barklem, and O'Mara (ABO) line damping theory (Barklem et al. 1998, and references therein), which allowed them to fit accurate damping constants to the profile of strong lines, turning these into reliable abundances indicators, an approach normally avoided in abundance analyses. They found [Fe/H] = 0.12 ± 0.06 for the iron abundance, which is in disagreement with most authors using the standard method, although in line with FM90. To bring home the point of the existing large disagreement between the various published results, one needs look no further than at the last entries of Table 1, all based on very high-quality data and state of the art methods. These disagreements in chemical composition lie beyond the confidence levels usually quoted by the authors. Moreover, the dispersion of the $T_{\rm eff}$ values found range between 300 K and 400 K, respectively, for component A and B.

Pourbaix et al. (1999) finish their paper thus: "we urge southern spectroscopists to put a high priority on α Centauri". Clearly, this very important stellar system is entitled to additional attention, fulfilling its utility as a reliable calibrator for theories of stellar structure and evolution, and taking full advantage of its tight observational constraints towards our understanding of our second closest neighbor and the atmospheres of cool stars. The widely differing results of the chemical analysis also cast doubt about the place of α Centauri in the galactic chemical evolution scenario. The goal of the present study is a simultaneous analysis of the two components of the system, obtaining their atmospheric parameters and detailed abundance pattern, providing an up-to-date comparative analysis of the different determinations, the methods used and their results.

This paper is organized as follows. In Sect. 2, we describe the data acquisition and reduction. In Sect. 3, we describe the spectroscopic derivation of the atmospheric parameters and Fe abundance, and compare them to other recent results from other techniques, discussing possible sources of discrepancies. The chemical composition pattern and its comparison to those of other authors, is outlined in Sect. 4. Section 5 is devoted to the analysis of the evolutionary state of the system, and Sect. 6 summarizes the conclusions.

2. Observations and line measurement

We performed observations, in 2001, with the coudé spectrograph, coupled to the 1.60 m telescope of Observatório do Pico dos Dias (OPD, Brasópolis, Brazil), operated by Laboratório Nacional de Astrofísica (LNA/CNPq). As both α Cen A and B are solar-type stars, the Sun is the natural choice as the standard star of a differential analysis. The expectation of this approach is that systematic errors in the measurement of line strengths, the representation of model atmospheres, and the possible presence of non-local thermodynamic Equilibrium (NLTE) effects, will be eliminated or at least greatly lessened if the standard and the analyzed object are sufficiently similar. We chose the moon as a sunlight surrogate to secure a solar flux spectrum. The slit width was adjusted to give a two-pixel resolving power R = 35 000. A 1800 l/mm diffraction grating was employed in the first direct order, projecting onto a 24 μm, 1024 pixels CCD. The exposure times were chosen to allow for a S/N ratio in excess of 1000. A decker was used to block one star of the binary system while exposing the other, and we ascertained that there was no significant contamination. The moon image, also exposed to very high S/N, was stopped orthogonally to the slit width to a size comparable to the seeing disks of the stars.

Nine spectral regions were observed, centered at $\lambda\lambda$ 5100, 5245, 5342, 5411, 5528, 5691, 5825, 6128, and 6242 Å, with spectral coverage of 90 Å each. The chemical species represented by spectral lines reasonably free from blending are Na I, Si I, Ca I, Sc I, Sc II, Ti I, Ti II,V I, Cr I, Cr II, Mn I, Fe I, Fe II, Co I, Ni I, Cu I, Y II, and Ba II. Additional data centered on the Hα spectral region, for the α Cen stars and moonlight, were secured in 2004, using a 13.5 μm, 4608 pixels CCD, integrated to $S/N \sim 500$ and with R = 43 000.

Data reduction was carried out by the standard procedure using IRAF[1]. After usual bias and flat-field correction, we

[1] *Image Reduction and Analysis Facility* (IRAF) is distributed by the National Optical Astronomical Observatories (NOAO), which is operated by the Association of Universities for Research in Astronomy (AURA), Inc., under contract to the National Science Foundation (NSF).

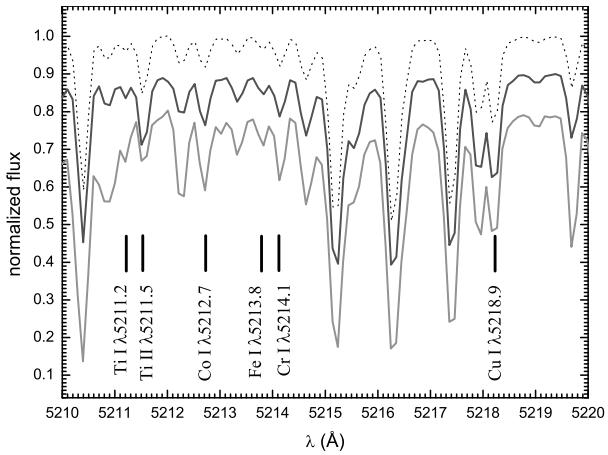

Fig. 1. Sample spectra of the Moon, employed as a proxy for the solar flux spectra, and α Centauri A and B. The nominal resolution is $R = 35\,000$, and the signal-to-noise (S/N) ratio is in excess of 1000. Some spectral lines measured for the spectroscopic derivation of the atmospheric parameters and the abundance analysis are indicated. The top, dotted spectrum is the Moon's, the dark gray one corresponds to α Cen A, and the light gray one to α Cen B. The α Cen spectra are arbitrarily displaced vertically. The stronger line blocking in α Cen B is apparent.

subtracted the background and scattered light and extracted one-dimensional spectra. No fringing was present in our spectra. The pixel-to-wavelength calibration was obtained from the stellar spectra themselves by selecting isolated spectral lines in the object spectra and checking for the absence of blends, the main screen for blends being the Solar Flux Atlas (Kurucz et al. 1984) and the Utrecht spectral line compilation (Moore et al. 1966). Gaussian fits were applied to the cores of the selected lines, and pixel-λ polynomial fits determined. For the short spectral selections individually reduced, a 2nd-order polynomial always sufficed, the average r.m.s. of the residuals being 0.005 Å or better. There followed the Doppler correction of all spectra to a rest reference frame.

Normalization of the continuum is a very delicate and relevant step in the analysis procedure, since the accuracy of line equivalent width (hereafter W_λ) measurements is very sensitive to a faulty determination of the continuum level. We selected continuum windows in the Solar Flux Atlas, apparently free from telluric or photospheric lines. We took great care in constantly comparing the spectra of the two α Cen components and the Sun, to ensure that a consistent choice of continuum windows was achieved in all three objects since the very strong-lined spectra of the α Cen stars caused continuum depressions systematically larger than in the Sun. A number of pixels was chosen in the selected continuum windows, followed by the determination of a low order polynomial fitting these points. The wavelength coverage of each single spectrum was in all cases sufficient to ensure an appropriate number of windows, with special attention given to the edge of the spectra. Sample spectra are shown in Fig. 1. As will be seen below, the errors of the atmospheric parameters derived directly from the spectra, and the element abundances of α Cen B, are greater than in α Cen A, probably due to a less trouble-free normalization of its strongly line-blocked spectrum, and to a better cancellation of uncertainties in the differential analysis.

For the determination of element abundances, we chose lines of moderate intensity with profiles that indicate little or no blending. To avoid contamination of telluric lines we computed for each spectrum, using cross-correlation techniques, the displacement $\Delta\lambda$ the telluric lines would show relative to their rest position λ_0, as given by the Solar Flux Atlas. We discarded photospheric lines closer than $2\Delta\lambda$ from a telluric line.

The equivalent widths were measured by fitting single or multiple (the latter when de-blending closely spaced lines) Gaussian profiles to the selected lines, using IRAF. The moderately high spectral resolution we chose was designed to guarantee that the instrumental profile dominates the observed profile, and therefore that purely Gaussian fits would adequately represent the observed line profiles. To test the representation of the solar flux spectrum by the moon, we also observed, with exactly the same setup, spectra of daylight, and the asteroid Ceres. A direct comparison of the moon, daylight, and asteroid W_λs showed perfect agreement between the three sets of measurements to better than 1% even for moderately strong lines. This lends confidence to our determination of solar gf-values based on W_λ measured off the moon spectra. The moonlight spectra was actually preferred due to its higher S/N ratio as compared to Ceres, for which no high-quality spectrum could be obtained in a reasonable exposure time. Also, daylight spectra may show W_λ systematic fill-in effects by up to 4%, as a combination of aerosol and Rayleigh-Brillouin effects (this effect depends on the observing angle and can be eliminated or minimized if care is applied, see Gray et al. 2000, for details). Even though no difference could be measured in our spectra, we considered it more prudent to use the moonlight spectrum as the solar proxy: it should be an accurate representation of the solar flux spectrum in the visible.

Even at our not-so-high resolution, lines stronger than ~50 mÅ begin to develop visible Voigt wings. To account for this effect, we performed a linear regression of our Gaussian moon W_λs against the W_λs measured off the Solar Flux Atlas by Meylan et al. (1993). These authors fitted Voigt profiles to a set of lines deemed sufficiently unblended to warrant the measurement of their true W_λs, and they should be a homogeneous and high-precision representation of the true line intensities. We then determined the correction necessary to convert our measurements to a scale compatible with the Voigt-fitted W_λs. A linear regression defines the correction to be applied to our measured W_λs to lessen systematic errors due to inadequate Gaussian profile fitting. As expected for non-saturated lines, we ascertained that a linear relationship suffices to describe the correction. The result is shown in Fig. 2, where the excellent correlation, with very small dispersion, is seen. The correction derived is

$$W_\lambda^{\rm Voigt} = (1.048 \pm 0.013) W_\lambda^{\rm moon}. \quad (1)$$

The rms standard deviation of the linear regression is 2.9 mÅ, regarding the Voigt W_λ as essentially error-free as compared to our data. This regression was applied to all our W_λ measurements. We take 2.9 mÅ as the 1σ uncertainty of our internal W_λ measurements.

3. Atmospheric parameters and Fe abundance

A solar gf-value for each spectral line was calculated from a LTE, 1D, homogeneous and plane-parallel solar model atmosphere from the NMARCS grid, as described by Edvardsson et al. (1993, see http://marcs.astro.uu.se; Gustafsson et al. 2008). The adopted parameters for the Sun were $T_{\rm eff} = 5780$ K, $\log g = 4.44$, [Fe/H] = +0.00 and $\xi_t = 1.30$ km s^{-1}, and we employed the W_λs measured off the moon

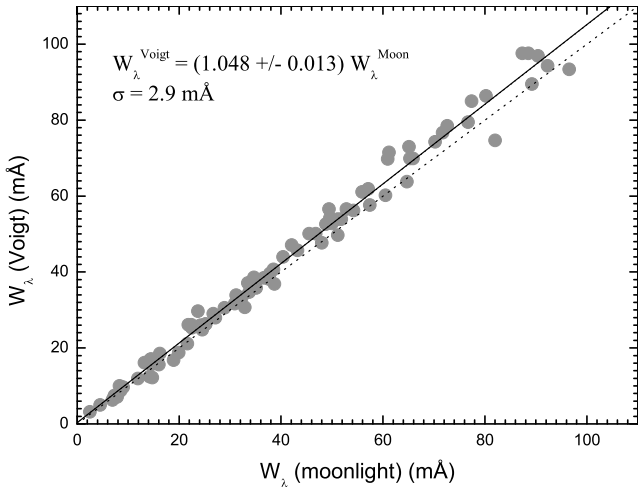

Fig. 2. A plot of Voigt-fitted W_λs from the Solar Flux Atlas, given by Meylan et al. (1993), against our Gaussian measurements, for the 84 common lines. The best fit (solid line) and the one-to-one line of identity (dotted line) are shown.

spectra, corrected to the Voigt scale. The adopted solar absolute abundances are those of Grevesse & Noels (1993). In a purely differential analysis such as ours, the absolute abundance scale is inconsequential. We provide in Table 2 (where A and B stand, respectively, for α Cen A and B) the details of all lines used. They include wavelength λ, excitation potential χ, the calculated solar $\log gf$ values, and the raw measured W_λs in the moon's, α Cen A and α Cen B spectra, prior to the correction to the Voigt system (Fig. 2). Hyperfine structure (HFS) corrections for the lines of Mg I, Sc I, Sc II, V I, Mn I, Co I, Cu I, and Ba II were adopted from Steffen (1985). del Peloso et al. (2005b) discuss the influence of adopting different HFS scales on abundance analyses of Mn and Co, concluding that it is small, particularly for metallicities not too far from the solar one, as compared to not using any HFS data. Therefore, the source of the HFS corrections is not an important issue on the error budget of our analysis, at least for Mn and Co. The other elements of our analysis requiring HFS have usually simpler structures (excepting Cu), and it is safe to conclude that the use of HFS has not introduced any important error.

The atmospheric parameters of the α Cen stars were determined by simultaneously realizing the excitation & ionization equilibria of Fe I and Fe II. For each star, we obtained the $T_{\rm eff}$ by forcing the Fe I line abundances to be independent of their excitation potential. We determined the surface gravity by forcing the lines of Fe I and Fe II to yield the same abundance. Lastly, we derived the microturbulence velocities ξ_t by forcing the lines of Fe I to be independent of their W_λs. The Fe abundance [Fe/H] (we use throughout the notation [A/B] = $\log N(\mathrm{A})/N(\mathrm{B})_{\rm star} - \log N(\mathrm{A})/N(\mathrm{B})_{\rm Sun}$, where N denotes the number abundance) is automatically obtained as a byproduct of this method. The solution thus obtained is unique for a given set of gf values, W_λs, and model atmospheres, being independent of the starting point and the iteration path. The spectrum synthesis code is originally due to Spite (1967), having been continuously up-dated in the last 40 years.

Formal errors are estimated as follows: for $T_{\rm eff}$, the 1σ uncertainty of the slope of the linear regression in the [Fe/H] vs. χ diagram yields the $T_{\rm eff}$ variation, which could still be accepted at the 1σ level. For the microturbulence velocity, the same procedure provides the 1σ microturbulence uncertainty in the [Fe/H] vs. W_λ diagram. For the metallicity [Fe/H], we adopt the standard deviation of the distribution of abundances derived from the Fe I lines. The error in $\log g$ is estimated by evaluating the variation in this parameter, which produces a disagreement of 1σ between the abundances of Fe I and Fe II, where we regarded the abundance offset as 1σ when its value was equal to the largest dispersion of the Fe abundances (usually that of Fe II). The results of this procedure are shown in Fig. 3, where we plot the iron abundances of α Cen A derived from lines of both Fe I and Fe II against the excitation potential and W_λs. The baseline of the Fe I lines is seen to be large both in W_λ and χ.

Additional effective temperatures were determined by fitting the observed wings of Hα, using the automated procedure described in detail in Lyra & Porto de Mello (2005). We have employed for the α Cen stars new spectroscopic data from the Observatório do Pico dos Dias, with the same resolution but greater signal-to-noise ratio than used by Lyra & Porto de Mello (2005). This procedure is shown in Figs. 4 and 5. We found $T_{\rm eff}$ = 5793 ± 25 K (α Cen A) and $T_{\rm eff}$ = 5155 ± 4 K (α Cen B). The moon spectrum is very well fitted by the parameters adopted for the NMARCS solar atmosphere model. The quoted standard errors refer exclusively to the dispersion of temperature values attributed to the fitted profile data points. This makes the uncertainty of the $T_{\rm eff}$ of α Cen B artificially very low, due to the high number of rejected points. An analysis of errors incurred by the atmospheric parameters assumed in the fitting procedure, plus the photon statistics (not including possible systematic effects produced by the modelling, see Lyra & Porto de Mello 2005, for a full discussion), points to an average error of ∼50 K in the $T_{\rm eff}$s determined from the Hα line. For the very low-noise spectra of these two stars, the expected errors would be slightly less, but the greater difficulty in finding line-free sections in the Hα profile of the severely blended spectrum of α Cen B offsets this advantage. For the latter, thus, the probable uncertainty should be closer to ∼100 K. The normalization procedure is a a relevant source of error for $T_{\rm eff}$s derived from Hα, as discussed by Lyra & Porto de Mello (2005): they found that a 0.2% error in the continuum level translates to ∼25 K in $T_{\rm eff}$.

As an external check on our normalization procedure, we compared Hα spectra of the Sun (moon) obtained from eight independent observing runs of Lyra & Porto de Mello (2005) and reduced independently, with the data of ABLC04, who performed a careful two-dimensional continuum normalization of the echelle spectra. Due to normalization problems in the FEROS/ESO (La Silla) spectra, these authors employed Hα spectra as a $T_{\rm eff}$ criterion only for the northern stars of their sample, which could be observed with the McDonald 2dcoudé spectrograph. So a direct comparison between the two sets of Hα spectra is not possible for the α Cen stars. We found, for the solar spectra, an average difference of only (−0.29 ± 0.39)%, as measured in those regions relevant to the $T_{\rm eff}$ determination. This assures us of the absence of important systematic errors in this respect. A comparison of the Hα normalized spectra is shown in Fig. 6. In the example shown, the mean difference between the two spectra (computed only for the line wing regions actually fitted) is −0.8 ± 0.7%, and it is the worst case of our comparison of the eight spectra.

Another check on the $T_{\rm eff}$ values of the two stars may be obtained from the IRFM scale of Ramírez & Meléndez (2005a). Ramírez & Meléndez (2005b) compare, for the two α Cen stars, direct $T_{\rm eff}$s, obtained from measured bolometric fluxes and angular diameters, with those determined from the IRFM method, as well those obtained from the application of their own $T_{\rm eff}$ (IRFM) scale to color indices and an adopted metallicity

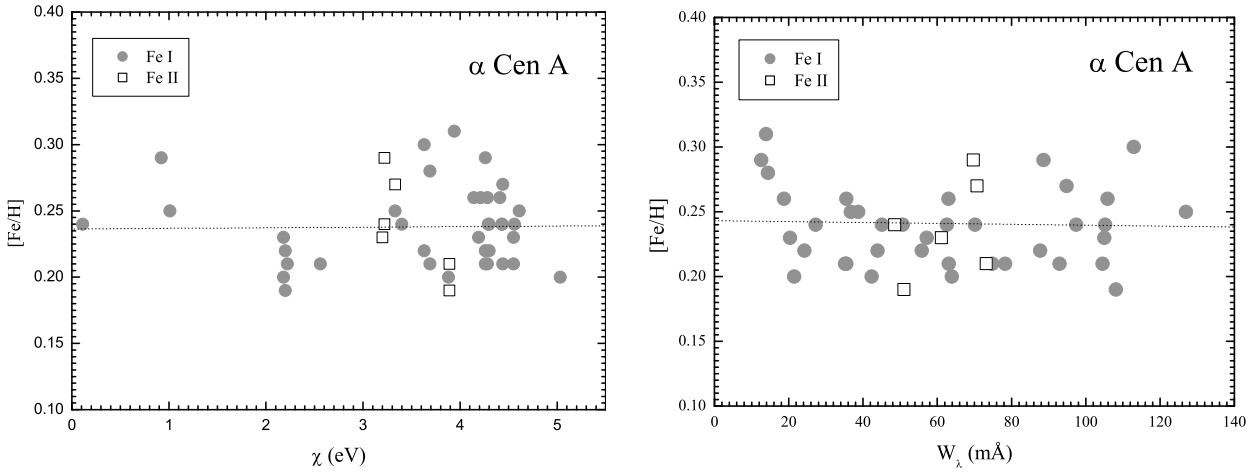

Fig. 3. *Left*. Fe I line abundances as a function of excitation potential χ in α Cen A. The dashed line is the regression of the two quantities. By forcing the angular coefficient to be null, we retrieve the excitation $T_{\rm eff}$ of the star. *Right*. Fe I line abundances as a function of equivalent width W_λ in α Cen A. A null angular coefficient provides the microturbulence velocity ξ_t. The ionization equilibrium between Fe I and Fe II constrains the surface gravity, and is realized simultaneously with the $T_{\rm eff}$ and ξ_t determinations.

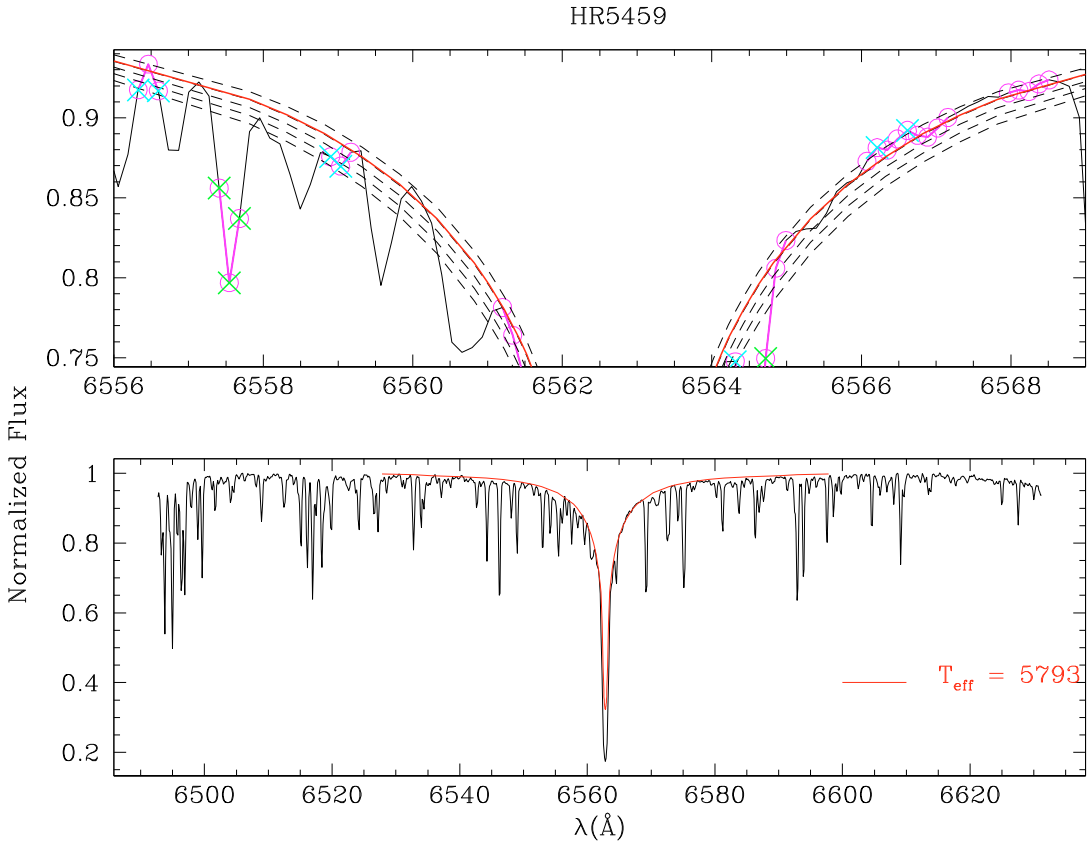

Fig. 4. Effective temperature determination by fitting theoretical profiles to the wings of Hα for α Cen A. *Upper panel*: crosses refer to pixels eliminated by the statistical test and 2σ criterion (see Lyra & Porto de Mello 2005, for details). The $T_{\rm eff}$ derived by the accepted pixels (open circles) is 5793 K. The corresponding best determined line profile is over-plotted (solid thick line) on the observed spectrum. The dashed lines are theoretical profiles, spaced by 50 K and centered in 5847 K, the spectroscopic $T_{\rm eff}$. *Lower panel*: the spectrum at a larger scale.

of [Fe/H] = +0.20, for both stars. Respectively, they find, for α Cen A, $T_{\rm eff}$ (direct) = 5771, $T_{\rm eff}$ (IRFM) = 5759 K and $T_{\rm eff}$ (calibration) = 5736 K; the corresponding values for α Cen B are, respectively, $T_{\rm eff}$ (direct) = 5178 K, $T_{\rm eff}$ (IRFM) = 5221 K and $T_{\rm eff}$ (calibration) = 5103 K. They adopt as weighted averages $T_{\rm eff}$ (α Cen A) = 5744 ± 72 K and $T_{\rm eff}$ (α Cen B) = 5136 ± 68 K. For α Cen A, a good agreement is found between this $T_{\rm eff}$ and our Hα one. Formally, there is also a reasonable agreement between this $T_{\rm eff}$ and our spectroscopic one. For α Cen B, however, the spectroscopic $T_{\rm eff}$ is significantly higher than those derived from Hα and the IRFM method.

Yildiz (2007) drew attention to often neglected *BVRI* (Cousins system) measurements of the system's components by Bessell (1990). It has long been considered risky to use color indices for the $T_{\rm eff}$ determination of very bright stars in which a variety of systematic effects are expected as compared to standard

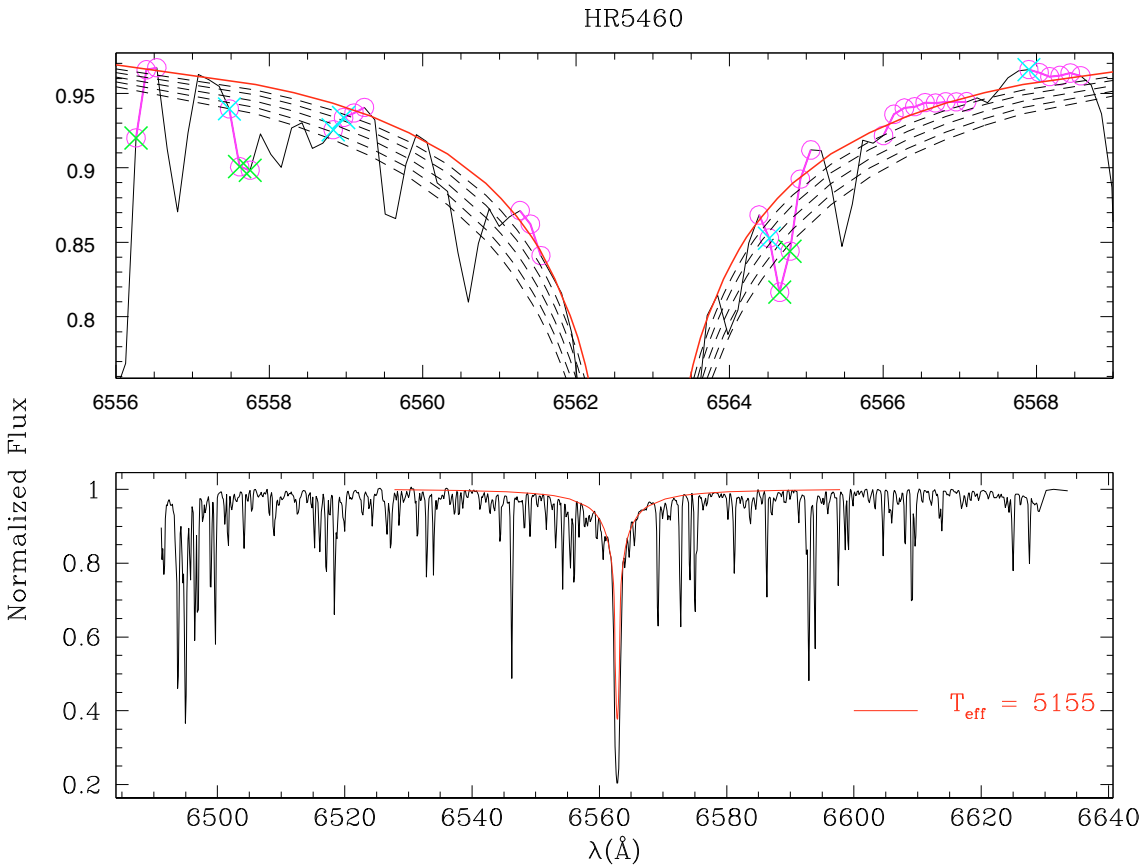

Fig. 5. The same as in Fig. 4 for α Cen B. The $T_{\rm eff}$ derived by the accepted pixels is 5155 K. The corresponding line profile is overplotted (solid thick line) on the observed spectrum. The dashed lines are theoretical profiles, spaced by 50 K and centered in 5316 K, the spectroscopic $T_{\rm eff}$. *Lower panel*: the spectrum at a larger scale.

stars of photometric systems, among which non-linearity, detector dead-time, and, in the case of α Cen, possible contamination by the companion (see Chmielewski et al. 1992, for a full discussion). Introducing Bessell's color indices into the Ramírez & Meléndez (2005b) calibrations, along with our metallicities (Table 3), we derive $T_{\rm eff}$ (α Cen A) = 5794 ± 34 K and $T_{\rm eff}$ (α Cen B) = 5182 ± 19 K, as a weighted average of the $(B-V)$, $(V-R)$ and $(V-I)$ color indices, the latter two in the Cousins system. These new photometric $T_{\rm eff}$ determinations, directly from the calibrations, agree well, for α Cen A, with both the Hα and the spectroscopic one. On the other hand, for α Cen B this determination lessens slightly, but does not eliminate, the disagreement between the spectroscopic $T_{\rm eff}$ and the other two. We must therefore state clearly that there is an offset between the spectroscopic $T_{\rm eff}$ of α Cen B and the other two $T_{\rm eff}$ determinations. These last figures, in a classical spectroscopic analysis of solar-type stars, would be regarded as "photometric" $T_{\rm eff}$s, to be compared to those obtained from other methods. Our results are all displayed in Table 3, where we also list the direct surface gravities resulting from the directly-observed radii and dynamical masses.

Valenti & Fischer (2005) have derived the atmospheric parameters of α Cen A and B by means of a different technique. They have directly fitted large sections of the observed spectra to synthetic ones, obtaining the atmospheric parameters (this technique also relies on the excitation & ionization equilibria of atomic species). Their analysis is differential with respect to the Sun, for which they adopted $T_{\rm eff}$ = 5770, [Fe/H] = +0.00 and $\log g$ = 4.44. They quote uncertainties of 44 K, 0.03 dex and 0.06 dex, respectively, for $T_{\rm eff}$, $\log g$ and [Fe/H]. Their results are $T_{\rm eff}$ = 5802 K, $\log g$ = 4.33 and [Fe/H] = +0.23, for α Cen A, and $T_{\rm eff}$ = 5178 K, $\log g$ = 4.56 and [Fe/H] = +0.21, for α Cen B. These figures are in good agreement, even within their very small claimed uncertainties, with our spectroscopic parameters, again, with the exception of the spectroscopic $T_{\rm eff}$ of α Cen B. Particularly, their $\log g$ values are in excellent agreement with the direct $\log g$ values of Table 3.

Frutiger et al. (2005) have also analyzed the spectra of α Cen A and B with a fundamentally different and promising technique. They have inverted high-resolution ($R \sim 10^5$), moderately high S/N (~250) spectra of the stars by means of a multi-component model photosphere. The components take into account rotational broadening, center-to-limb variations and vertical and horizontal flows of surface elements, such as granules and inter-granular areas. In this approach, the full line profile is used to constrain the temperature stratification of the atmosphere, as well as the velocity fields (Allende-Prieto et al. 1998). The technique is rather model-dependent, however, and should be compared with classical spectroscopic analyses with caution. For the 3-component models, the ones they favor, $T_{\rm eff}$s and [Fe/H] substantially lower than those found by us are obtained (their Table 4). For α Cen A, they favor $T_{\rm eff}$ = 5705 K, $\log g$ = 4.28 ± 0.03 and [Fe/H] = +0.08 ± 0.02 (we have converted their abundances from absolute to relative values with respect to the Sun, which they also analyzed with the same techniques. Their analysis, in this sense, may also be considered as differential). For α Cen B, the results are $T_{\rm eff}$ = 5310 K, $\log g$ = 4.74 ± 0.02 and [Fe/H] = +0.05 ± 0.01.

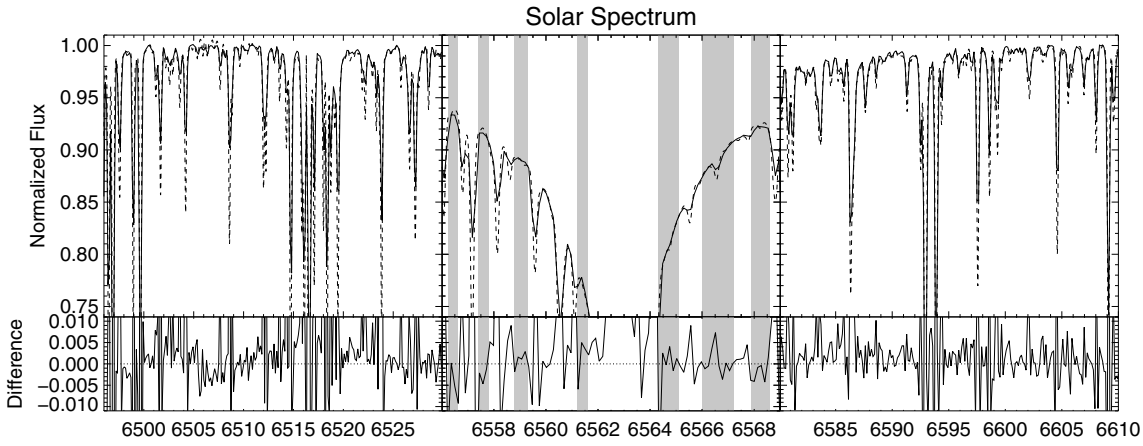

Fig. 6. A comparison of the normalization of our Hα spectrum of the Sun (moon) with that of ABLC04. The large differences in the telluric lines are apparent. The left and right panels depict the regions outside the Hα profile, which were used for the continuum normalization. In the central panel, we depict, as the shaded gray areas, the wavelengths of the wing profile used for the $T_{\rm eff}$ determination. Note that the abscissa is truncated to show only the most relevant portions of the spectra, the blue and red limits, which set the normalization scale, and those used directly for the fit of the line wings.

Table 3. The atmospheric parameters of α Cen A and B derived from various methods. The mean $T_{\rm eff}$ is weighted by the inverse variances (see text).

	$T_{\rm eff}$ (K) excitation	$T_{\rm eff}$ (K) Hα	$T_{\rm eff}$ (K) photometric	$T_{\rm eff}$ (K) weighted mean	$\log g$ ionization	$\log g$ direct	[Fe/H]	ξ_t(km s^{-1})
α Cen A	5847 ± 27	5793 ± 50	5794 ± 34	5824 ± 26	4.34 ± 0.12	4.307 ± 0.005	+0.24 ± 0.03	1.46 ± 0.03
α Cen B	5316 ± 28	5155 ± 100	5182 ± 19	5223 ± 62	4.44 ± 0.15	4.538 ± 0.008	+0.25 ± 0.04	1.28 ± 0.12

It is not straightforward to determine the uncertainties of their $T_{\rm eff}$ values, since they only quote the uncertainty of this parameter as derived by a weighted average of the σT^4 fluxes of each atmospheric component, weighted by the filling-factors, by means of the Eddington-Barbier relation applied to a grey atmosphere. The $T_{\rm eff}$s we quoted are the ones they computed from the flux spectra obtained from their temperature stratifications fed into an ATLAS9 model, for which they provided no formal uncertainty. The uncertainties of their $T_{\rm eff}$s within the Eddington-Barbier approximation, are, respectively, 130 K and 67 K for α Cen A and B. Within these error bars, then, their $T_{\rm eff}$s resulting purely from the inversion procedure (letting all parameters free) may be regarded as compatible with ours. Their metallicities, however, are significantly lower. They also found a very high $\log g$ for α Cen B, prompting them to attempt a larger number of inversions this for component, first fixing $\log g$ = 4.48 dex, which led to a reduced $T_{\rm eff}$ = 5154 K with no appreciable change in metallicity, and then fixing the rotational velocity, which produced $T_{\rm eff}$ = 5260 K, again with no significant impact on metallicity, and a new $\log g = 4.68 \pm 0.05$.

The $T_{\rm eff}$s favored by the inversion method of Frutiger et al. (2005) add to a complex situation. They seem to be in good agreement with our spectroscopic $T_{\rm eff}$ for α Cen B when all parameters are independently derived from the inversion method, but the agreement switches to one with the Hα and photometric $T_{\rm eff}$s, when the surface gravity is fixed. All [Fe/H] values they obtain are lower than ours. For α Cen A, their surface gravity is in good agreement with ours and the direct one. It is difficult, however, to reconcile their surface gravity for α Cen B with our spectroscopic one, and the direct one given in Table 3. It is not clear whether their results can be directly compared to ours, given the difference in approach. These authors discuss the possibility of improving their technique by higher resolution spectra: they remark on the difficulty of disentangling effects of rotation, macro-turbulence, granulation, and instrumental profile. This sophisticated approach can lead to substantially improved constraints in the derivation of the atmospheric parameters of solar-type stars, leading to increased physical insight on the shortcomings of 1D, static atmospheric models.

Table 4. The abundance pattern of the α Cen stars.

element	α Cen A [X/Fe]	σ	α Cen B [X/Fe]	σ	Δ
Na	+0.14	–	+0.25	–	0.03
Mg	0.00	–	+0.04	–	0.03
Si	0.00	0.06	0.00	0.05	0.05
Ca	+0.03	0.03	+0.09	0.08	0.03
Sc	0.00	0.02	+0.01	0.07	0.06
Ti	−0.01	0.04	+0.19	0.14	0.06
V	+0.02	0.05	+0.21	0.09	0.07
Cr	0.00	0.06	+0.06	0.09	0.06
Mn	+0.07	0.01	+0.19	0.06	0.04
Co	0.00	0.06	+0.06	0.07	0.07
Ni	+0.10	0.07	+0.11	0.05	0.04
Cu	+0.10	–	+0.10	–	0.04
Y	−0.09	0.05	−0.09	0.08	0.07
Ba	−0.13	0.05	−0.16	0.08	0.06

3.1. Systematic offsets between spectroscopic, Balmer line and photometric $T_{\rm eff}$ scales

The study of the atmospheric parameters collected in Table 1 reveals an interesting pattern, if one again considers only the analyses published since the 90s, invariably based on high S/N spectra acquired with solid-state detectors. For α Cen A, the works

employing the Fe I/Fe II criterion, alone or combined with another method, obtained $T_{\rm eff}$s generally higher than those derived exclusively from photometry (excepting the result of FM90, which is one of the lowest and applied the excitation & ionization approach). Thus, the present work, Santos et al. (2004) and Neuforge-Verheecke & Magain (1997) found the highest $T_{\rm eff}$s, while ABLC04, relying only on photometry, derived the lowest $T_{\rm eff}$. Doyle et al. (2005) also used the stellar luminosity and radius to derive $T_{\rm eff}$ and found a value lower than the spectroscopic ones, but for the FM90 analysis. ABLC04 reported good agreement of their photometric $T_{\rm eff}$s with those derived from the Hβ profiles. Interestingly, they also found an offset of ~120 K between their $T_{\rm eff}$s and the ones of Kovtyukh et al. (2003), the latter being the higher. Kovtyukh et al. (2003) derived $T_{\rm eff}$s by the line-depth ration method (Gray & Johanson 1991), and their $T_{\rm eff}$s were actually calibrated by spectroscopic ones. The pattern just discussed suggests that the spectroscopic $T_{\rm eff}$ scale is indeed hotter than the photometric and Balmer line one, and that the latter two are in generally good agreement. The situation for α Cen B is unfortunately much less clear: there are less analyses, and the authors employed a more restricted set of criteria. Nevertheless, the lowest $T_{\rm eff}$ is again due to photometric methods (ABLC04), the highest one in this case corresponding to the Hα-derived $T_{\rm eff}$ of Chmielewski et al. (1992).

A disagreement between photometric and spectroscopic $T_{\rm eff}$ scales has been recently pointed out by a number of authors. Ramírez et al. (2007) discussed how the Fe I/Fe II ionization equilibrium is not realized in cool stars when an IRFM $T_{\rm eff}$ scale is applied, in the derivation of oxygen abundances from the λ7774 triplet lines. Their sample is large, and they convincingly show (their Fig. 5) that the $T_{\rm eff}$ offset between the IRFM and the spectroscopic scales is significant for $T_{\rm eff} \sim 5000$ K (a reasonable agreement was found for $T_{\rm eff} \sim 6000$ K). They note that Ramírez & Meléndez (2004) found the same offset, as did Santos et al. (2004), Yong et al. (2004) and Heiter & Luck (2003). Yong et al. (2004) suggested that non-LTE effects, shortcomings of the model atmosphere representation for cool stars, or as yet unidentified effects, might be responsible for the discrepancy. Ramírez et al. (2007), however, note that Santos et al. (2005) reported good agreement between IRFM and spectroscopic $T_{\rm eff}$ scales. Adding to this complex picture, Casagrande et al. (2006), in the derivation of their own IRFM $T_{\rm eff}$ scale, also found good agreement between spectroscopic and IRFM $T_{\rm eff}$s. They argue that the disagreement reported by other authors might be due, at least in part, to uncertainties in the different absolute flux calibrations adopted, and suggest that additional direct angular diameter measurements for a well-chosen sample of G and K dwarfs might go a long way towards clarifying the disagreement of the $T_{\rm eff}$ scales.

The results of Casagrande et al. (2006) were essentially backed by the $T_{\rm eff}$ scale of Masana et al. (2006). The latter employed a variation of the IRFM method, in which the stellar energy distributions were fitted, from the optical to the IR, to synthetic photometry computed from stellar atmosphere models. They found their results only slightly offset from the IRFM results. The offset, at ~30 K, was deemed to be small, and these authors optimistically assert that their $T_{\rm eff}$ scale agrees with the spectroscopic one for FGK dwarfs and subgiants, such that $T_{\rm eff}$s for this class of stars may be regarded as accurate within ~1% or better.

The consistency of the different $T_{\rm eff}$ scales is sought as an important confirmation that 1D, plane-parallel, static and LTE model atmospheres adequately represent cool stars, if not in the absolute, at least in the relative sense, provided that the Sun can be accurately placed in the stellar context. The solar placement in the Fe I/Fe II excitation & ionization equilibria and Balmer line $T_{\rm eff}$ scale is obtained by the observation of solar flux spectra. An accurate photometric placement of the Sun in the corresponding $T_{\rm eff}$ scale, however, is a difficult task still beset with large uncertainties (see, e.g., Holmberg et al. 2006, for an up-to-date discussion). These three $T_{\rm eff}$ scales actually gauge rather dissimilar physical quantities. The excitation & ionization $T_{\rm eff}$ is obtained by matching models to observed spectral line intensities. The Balmer line $T_{\rm eff}$ measures the temperature stratification of the atmosphere, which is mapped onto the line wings by the depth-dependence of the source-function. The photometric $T_{\rm eff}$ must reproduce the stellar flux distribution in a large wavelength regime, and is the one most directly tied to the fundamental definition of effective temperature (Böhm-Vitense 1981). As long as the consistency between these scales is realized no better than within ~150 K, the $T_{\rm eff}$ of cool dwarfs and subgiants will remain uncertain by this amount at the very least.

Non-LTE and other possibly more complex effects have repeatedly been blamed for offsets between spectroscopically- and photometrically-derived atmospheric parameters in cool stars. Schuler et al. (2006), in their analysis of Hyades dwarfs, reported a systematic offset of the oxygen abundances derived from the λ7774 triplet lines, for $T_{\rm eff} < 5450$ K, in the opposite sense of the NLTE expectations. They tentatively suggest that chromospheric activity might be at least partially responsible for the offset, an explanation also concurred by Morel & Micela (2004), though the latter propose that model atmosphere pitfalls might be also present. Schuler et al. (2006) reinforce this interpretation in an analysis of the λ6300 [OI] line in the very active Hyades stars, reporting offsets between Fe I/Fe II abundances which increase as $T_{\rm eff} \leq 5000$ K. It should be emphasized that high chromospheric activity is unlikely to be a source of the $T_{\rm eff}$ discrepancy of α Cen B, since both components of the system are inactive stars, which probably implies that the problem is more complex. We also draw attention to the result of Shchukina & Trujillo-Bueno (2001), who found an offset of the Fe I/Fe II abundances of the Sun. They interpret this offset as well explained by NLTE effects amounting to 0.07 dex for Fe I, the best fit Fe abundance for a LTE analysis being the lower by this amount. They assert that a full 3D, NLTE model atmosphere formulation is able to bring the solar photospheric Fe abundance in line with the meteoritic one, at $\log N({\rm Fe}) = 7.50$ (in the usual scale where $\log N({\rm H}) = 12.00$). The main cause of the offset is the overionization of Fe I, and the larger errors are seen in the W_λs of low excitation lines, which are weaker in the NLTE case.

It is interesting to note that this effect, in a classical LTE model atmosphere analysis, would result in the overabundance of the high excitation Fe I lines, an effect naturally interpreted as too low a $T_{\rm eff}$ being attributed to the model. This is exactly the condition necessary for a 1D, LTE analysis to lead to the high spectroscopic $T_{\rm eff}$ that we obtained. Forcing the Fe I/Fe II abundances into agreement in a LTE analysis would indeed call for a higher $T_{\rm eff}$, to a first approximation, by ~100 K, a value similar to the difference between our spectroscopic and Hα/photometric $T_{\rm eff}$s of α Cen B. We suggest that the similarity in atmospheric parameters between α Cen A and the Sun, in the context of a differential analysis, led to a good agreement between the three $T_{\rm eff}$ criteria for the former. For α Cen B, a much cooler object, an imperfect cancellation of the presence of NLTE effects is probably the reason why the three different $T_{\rm eff}$ criteria do not agree.

Even if the presence of NLTE effects and other problems can be established, one must keep in mind that other uncertainties are present in the photometric and Hα $T_{\rm eff}$ scales, as discussed

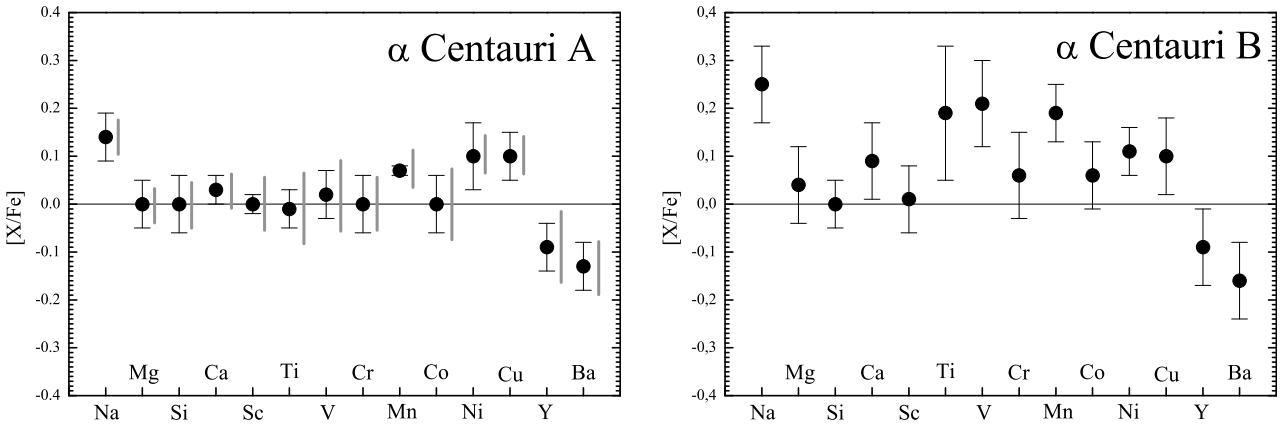

Fig. 7. The abundance pattern of α Cen A & B. The uncertainty bars are the dispersions of the abundances given by the element lines. The gray bars beside the data points in the α Cen A plot correspond to the total compounded errors arising from the atmospheric parameters and the W_λs (see Table 4).

above. It would be very valuable to extend the novel approaches of Valenti & Fischer (2005) and Frutiger et al. (2005) to additional stars for which stringent observational constraints are available, to quantify how discrepancies of the type discussed here occur for objects with atmospheric parameters increasingly different from the Sun's. At present, we can state that it is likely that our spectroscopic $T_{\rm eff}$ for α Cen B is more uncertain, and systematically higher, that the other two determinations. This conclusion is, however, drawn in the context of a confusing picture. Additional work is clearly necessary before a definitive judgment can be passed on the consistency between the excitation & ionization, Balmer line, and photometric $T_{\rm eff}$ scales can be reached.

Notwithstanding the discrepancies, if we follow an usual practice in spectroscopic abundance analysis, which obtain atmospheric parameters with more than one criterion, mean $T_{\rm eff}$s for the α Cen stars can be calculated from the values of Table 3, averaged by their inverse variances. The results are $T_{\rm eff}$ (α Cen A) = 5824 ± 27 K and $T_{\rm eff}$ (α Cen B) = 5223 ± 62 K, where the quoted uncertainties are the standard deviations of the average, and do not reflect external and systematic errors. Good agreement between our ionization surface gravities, and those directly determined from measured masses and radii, within the errors, for both stars, is realized.

4. Abundance pattern

The abundances of the other elements were obtained with the adopted atmospheric model of each star, corresponding to the spectroscopic $T_{\rm eff}$s, and the $\log g$, [Fe/H] and ξ values as given in Table 3. Average abundances were calculated by the straight mean of the individual line abundances. For Sc, Ti, and Cr, good agreement, within the errors, was obtained for the abundances of the neutral and singly ionized species, and thus these species confirm the Fe I/Fe II ionization equilibria. The results are given in Table 4 and Fig. 7 as [X/Fe] relative to the Sun. In Table 4, the first two columns give the [X/Fe] ratios with the corresponding observed dispersions of the line abundances, for those elements with three or more available lines, for α Cen A. The next two columns give the corresponding data for α Cen B. The fifth column provides the total uncertainty of the [X/Fe] ratios corresponding to errors in $T_{\rm eff}$, $\log g$, [Fe/H], ξ and W_λ, respectively, of 30 K, 0.12 dex, 0.04 dex, 0.03 km s^{-1} and 2.9 mÅ, composed in quadrature (the latter enters twice, see Sect. 3).

In Fig. 7, the error bars are merely the internal dispersion of the individual line abundances. For Na I, Mg I, Cu I, and Ba II, the dispersions refer to the difference between the abundances of the two available lines for each element. Na is seen to be overabundant, while a solar pattern is seen from Mg to Co, but for an excess of Mn. Ni and Cu are also overabundant. Some doubt can be cast about Ti and V, since they seem overabundant in α Cen B although solar in α Cen A. The slow neutron capture elements Y and Ba are in clear deficit. The bigger uncertainty bars seen in α Cen B are probably a result of a less accurate normalization of the spectra of a cooler star, and may also be due to its less accurate atmospheric parameters. We may conclude that there is a good consistency between the abundance patterns of the two stars, except for the Ti I and V I abundances, but these can still be accomodated by the larger error bars for α Cen B at the 2σ level.

In Fig. 7, the vertical dark grey bars besides the data points of the abundance pattern of α Cen A are the composed rms uncertainties, for each element, calculated by varying the spectroscopic atmospheric parameters of α Cen A by the corresponding uncertainties of Table 3. To this calculation, we added the abundance variations caused by summing to all W_λs the 2.9 mÅ uncertainty of the correction of Fig. 2. This W_λ uncertainty enters twice: once for the uncertainty in the corrected moon W_λs, reflecting onto the solar $\log gf$s, and another one due to stellar W_λ themselves. In Fig. 7, it is apparent that the abundance variations due to the uncertainties in the atmospheric parameters and W_λs are comparable to the observed dispersions of the line abundances for α Cen A. For α Cen B, the line abundance dispersions are generally larger, probably due to its more uncertain W_λs, but also, as discussed above, possibly owing to its larger $T_{\rm eff}$ difference from the standard object (the Sun) and its more uncertain atmospheric parameters.

Our abundance pattern for α Cen A is clearly the most reliable of the pair, and is directly compared to those of other authors in Fig. 8. Only abundances represented by more than one spectral line are shown. The observed dispersion is comparable to the uncertainties normally quoted in a spectroscopic analysis. Only for the light elements between Mg and Ti is a larger disagreement observed, in this case due to the analysis of ABLC04, in which abundances are higher than in the bulk of other data by ~0.2 dex. For the elements heavier than V, essentially all data agree that V and Cr have normal abundance ratios, that Mn, Co, Ni, and Cu are enhanced, and all heavy elements from Y to Eu are deficient in the abundance pattern of α Cen A with respect to

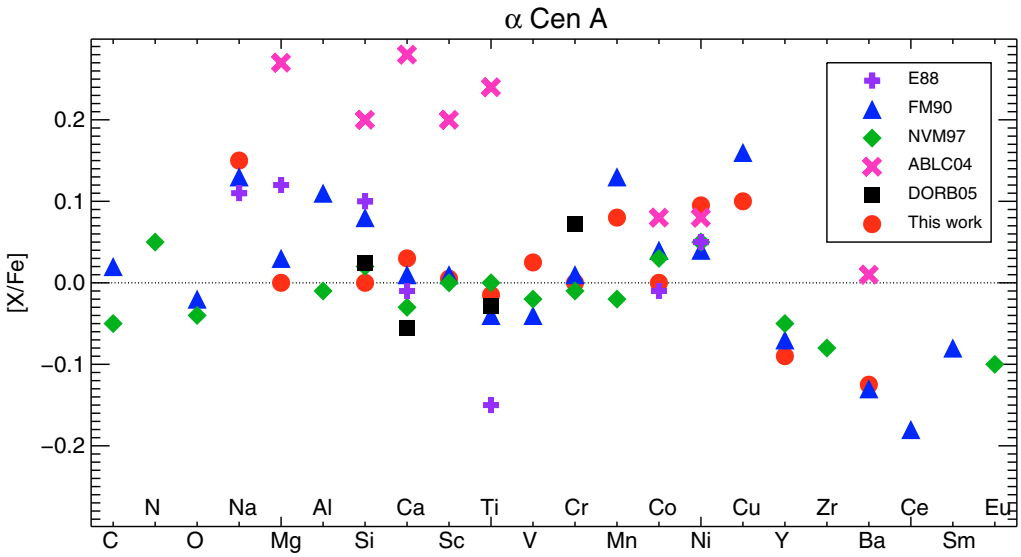

Fig. 8. A comparison of the [X/Fe] abundance pattern of α Cen A derived by different authors. E88 stands for Edvardsson (1998). Only elements for which abundances are based on more than one line are included. Apart from the ABLC04 results, which point to excesses of nearly all elements with respect to the Sun, most published data imply an abundance pattern in which C, N, O, Ca, Sc, V, and Cr are normal; Na, Mn, Co, Ni, and Cu are enhanced; Mg, Al, and Si are possibly enhanced; and Ti and all elements heavier than Y are under-abundant.

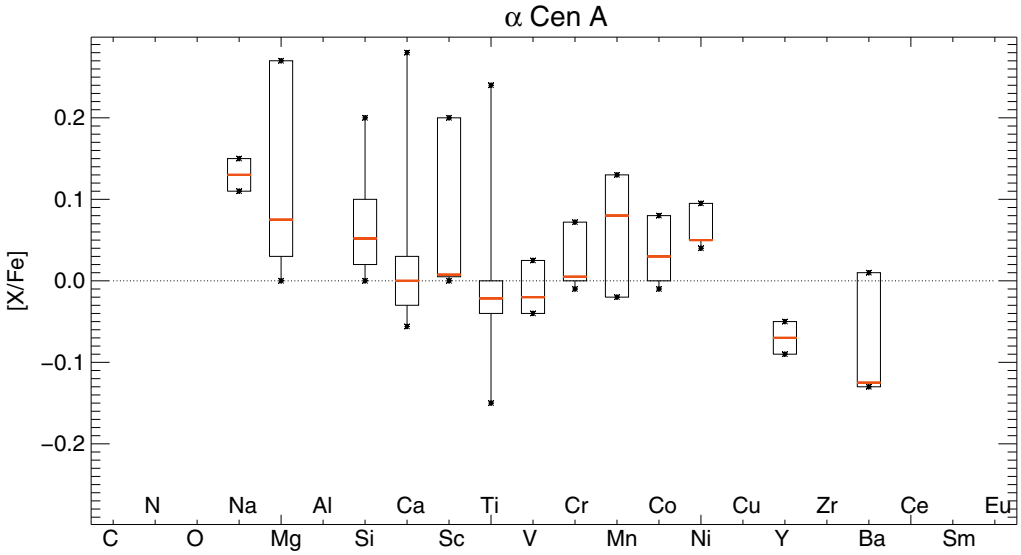

Fig. 9. The same as Fig. 9, but averaging the [X/Fe] abundances of the elements with published data from at least three authors. The boxes comprise 50% of the data points, and are centered at the mean. The horizontal dashes inside the boxes mark the median. The whiskers mark the maximum and minimum values. In this more stringent statistical analysis of the available data, Na, Mg, Si, Mn, Co, and Ni are enhanced; Ca, Sc, Ti, V, and Cr are normal; Y and Ba are under-abundant.

the Sun, with the sole exception of Ba, for which ABLC04 found a normal abundance. The available literature data also suggests that the C, N, and O abundance ratios of α Cen A are solar.

This statistical analysis can be extended if we regard only the elements for which at least three independent studies provided data. This is shown in Fig. 9, for a more select sample of elements. We may conclude, with somewhat greater robustness, considering the number of abundance results, that Na, Mg, Si, Mn, Co, and Ni are over-abundant; that Ca, Sc, Ti, V, and Cr have solar abundance ratios; and that Y and Ba are over-deficient in the abundance pattern of α Cen with respect to the Sun.

The high metallicity of the α Cen system, and its space velocity components (U, V, W) (km s^{-1}) = (−24, +10, +8) (Porto de Mello et al. 2006, all with respect to the Sun) place it unambiguously as a thin disk star. We next analyze its abundance ratios, for the elements with more reliable data, as compared to recent literature results for metal-rich stars. Bensby et al. (2003, hereafter BFL) analyzed 66 stars belonging to the thin and thick disks of the Milky Way, deriving abundances of Na, Mg, Al, Si, Ca, Ti, Cr, Fe, Ni, and Zn. Bodaghee et al. (2003, hereafter BSIM) studied a sample of 119 stars, of which 77 are known to harbor planetary companions, deriving abundances of Si, Ca, Sc, Ti, V, Cr, Mn, Fe, Co, and Ni. The data of the latter study comes from the Geneva observatory planet-search campaign (e.g., Santos et al. 2005). Since they concluded that planet-bearing stars merely represent the high metallicity extension of the abundance distribution of nearby stars, their full sample can be used to adequately represent the abundance ratios of metal rich stars, without distinction to the presence or absence of low mass companions. These two works have in common

the important fact that they sample well the metallicity interval +0.20 < [Fe/H] < +0.40, an essential feature for our aim.

The elements in common between the two abundance sets are Si, Ca, Ti, Cr, and Ni. It can be concluded (Fig. 13 of BFL, Fig. 2 of BSIM) that, in [Fe/H] ≥ +0.20 stars, Ca is under-abundant, Ti is normal and Ni is enhanced. For Si, BFL suggest abundance ratios higher than solar, while BSIM found a normal abundance. For Cr, the data of BSIM suggests abundance ratios lower than solar, while BFL found solar ratios. For the elements not in common in the two studies, Na, Mg, Al, Sc, V, Mn, and Co are found to be enhanced in [Fe/H] ≥ +0.20 stars, while Zn has normal abundance ratios.

An interesting feature of the α Cen abundance pattern is the under-abundance in the elements heavier than Y, which could be reliably established for Y and Ba (Fig. 9). This result is confirmed by Bensby et al. (2005), who found both for Y and Ba lower than solar abundance ratios for metal rich thin disk stars. Another interesting feature, the excess of Cu (found by us and FM90), can be checked with the recent results of Ecuvillon et al. (2004), who also obtain for [Fe/H] ≥ +0.20 stars an average [Cu/Fe] ~ 0.1 dex.

Merging our evaluation of the abundance pattern of α Cen A, from the available independent analyses, with the previous discussion, we conclude that α Cen A is a normal metal-rich star in its Na, Mg, Si, Ti, V, Cr, Mn, Co, and Ni abundances. The result for Ca is inconclusive, and only for Sc does its abundance diverge from the BFL/BSIM data in that its normal abundance ratio contrasts with the overabundance found for [Fe/H] ≥ +0.20 stars by BSIM. It seems reasonably well established then that the α Cen system is composed of two normal metal rich stars when regarded in the local disk population.

5. Evolutionary state

An important outcome of the present analysis is to establish if the derived atmospheric parameters, coupled to high-quality parallaxes, allow a consistent determination of the masses and ages of the α Cen system in a traditional HR diagram analysis, matching the stringent constraints posed by the orbital solution and seismological data. In Fig. 10, we plot the position of the α Cen components in the theoretical HR diagram of Kim et al. (2002) and Yi et al. (2003), corresponding to its exact metallicity and a solar abundance pattern. The bolometric corrections were taken from Flower (1996), and in calculating the luminosities the Hipparcos (ESA 1997) parallaxes and visual magnitudes were used. Evolutionary tracks and isochrones from different authors (e.g., Girardi et al. 2000; Charbonnel et al. 1999; Schaller et al. 1992) were also tested, and good agreement between the different tracks was found, to better than ~50 K, for the position of both α Cen components. This is an expected result, given that the Sun is generally used to calibrate these models. The solar mass, radius, and age provide a zero point to the models and allow for a solution as a function of the adopted mixing-length of the convection theory (still a free parameter) and the initial helium abundance. Thus, differences between the models can be substantial in the treatment of stars that are very different from the Sun (e.g., Lyra et al. 2006), but good agreement for solar-type stars is a natural outcome of this procedure. The conclusions drawn below, then, are essentially model-independent, at least for the $T_{\rm eff}$ and luminosity intervals involved here.

The $T_{\rm eff}$ values and error bars in the diagram are those of the weighted mean of Table 3. From the diagram, masses of $M_{\rm A} = 1.13 \pm 0.01$ and $M_{\rm B} = 0.89 \pm 0.03$ can be derived, and agree well with the orbital solution of Pourbaix et al. (2002).

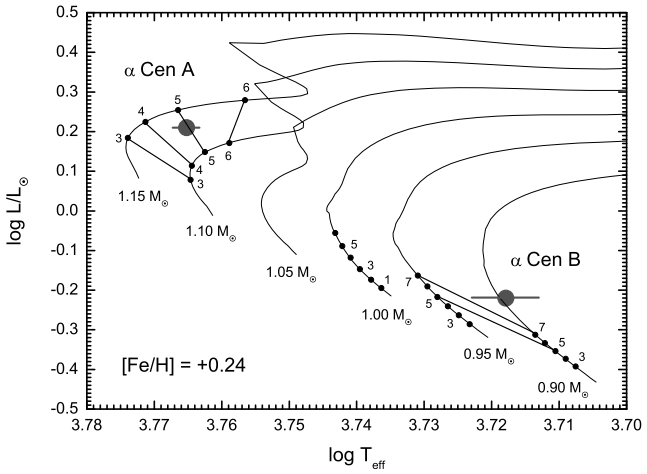

Fig. 10. The evolutionary state of the α Cen system. The stars are plotted in the HR diagram superimposed to the isochrones and evolutionary tracks of Kim et al. (2002) and Yi et al. (2003). The horizontal error bars refer to the uncertainties of Table 3. The actual uncertainties in the luminosities are smaller than the symbol size. The tracks are labelled with masses in solar units. The numbers alongside the tracks are ages in Gyr. The thin solid lines between the tracks join points with the same age.

The age of α Cen A can be relatively well constrained to the interval of 4.5 to 5.3 Gyr (1σ), again, in good agreement with the seismological results of Yildiz (2007), Eggenberger et al. (2004), Miglio & Montalbán (2005) and Thoul et al. (2003), within the quoted uncertainties. We conclude that, adopting the average $T_{\rm eff}$s and [Fe/H] found in this work, the position of α Cen A in up-to-date theoretical HR diagrams can be reconciled both with seismological and dynamical data. Despite its higher mass and its being (probably) older than the Sun, the higher metallicity slows the evolution to the point that the star has not yet reached the "hook" zone of the HR diagram, thus enabling a unique age solution through this type of analysis.

Concerning α Cen B, it is also apparent in Fig. 10 that its position cannot be reconciled, within 1σ, with an age near 5 Gyr, as was possible for α Cen A. However, an upward revision of only ~60 K would bring its position in agreement with a track of 0.93 solar mass (the dynamical value), and an age of ~5−8 Gyr. Given the uncertainties discussed in Sect. 3, along with the probable effect of systematic errors in the $T_{\rm eff}$ determination of α Cen B, this is not outside the 2σ confidence interval of the results. We conclude that α Cen A has its position in the theoretical HR diagram well matched by up-to-date models, within the uncertainties of the determination of its atmospheric parameters, and also within the small differences, in this $T_{\rm eff}$ and luminosity regime, between different grids of evolutionary models. For α Cen B, however, the larger $T_{\rm eff}$ uncertainty precludes a more stringent assessment of a match between its evolutionary mass and age and the results from the dynamical solution and asteroseismology. Further data are still necessary to allow for a more definitive conclusion on this issue. If indeed its spectroscopic $T_{\rm eff}$ is systematically offset, the mean $T_{\rm eff}$ we derived would decrease and displace its position on the HR diagram to the right, forestalling a match with the age of α Cen A. For a better understanding of the onset of possible NLTE effects in cool stars, and the hindrance thus incurred in the determination of their atmospheric parameters, it would be interesting to perform further analyses of such objects for which high-quality spectra could be secured, and the relevant

observational constraints made at least partially available. Interesting bright, nearby K-dwarf candidates for such an enterprise are ϵ Eri, 36 and 70 Oph, o^2 Eri and σ Dra.

6. Conclusions

We have undertaken a new detailed spectroscopic analysis of the two components of the α Centauri binary system, and have attempted an appraisal of the many discordant determinations of its atmospheric parameters and abundance pattern, and of the sources of errors in their determination. We derived purely spectroscopic atmospheric parameters, from $R = 35\,000$ and $S/N > 1000$ spectra, in a strictly differential analysis with the Sun as the standard. We obtained $T_{\rm eff\ A} = 5847 \pm 27$ K and $T_{\rm eff\ B} = 5316 \pm 28$ K from the spectroscopic analysis, and $T_{\rm eff\ A} = 5824 \pm 26$ K and $T_{\rm eff\ B} = 5223 \pm 62$ K from the average of spectroscopic, Hα and photometric $T_{\rm eff}$s. We derived [Fe/H] $= +0.24 \pm 0.03$ dex for the system. The spectroscopic surface gravities, $\log g_{\rm A} = 4.34 \pm 0.12$ and $\log g_{\rm B} = 4.44 \pm 0.15$, are a good match to those determined from directly measured masses and radii. Good agreement, in both components, is found between the photometric $T_{\rm eff}$ and the one resulting from the fitting of the wings of Hα. For α Cen A, these two $T_{\rm eff}$s also agree with the spectroscopic one. However, for α Cen B, the spectroscopic $T_{\rm eff}$ was found to be significantly higher, by ~140 K, than the other two. A comparison of the published $T_{\rm eff}$s for the system in the last 20 years roughly support a spectroscopic $T_{\rm eff}$ scale hotter than the ones owed to photometric methods or the fitting of Balmer lines.

A comparison with recent results from other techniques revealed an unclear picture. Atmospheric parameters for the α Cen stars derived by Valenti & Fisher (2005) by fitting directly synthetic spectra to a large spectral coverage, agree well with our determinations, but for the spectroscopic $T_{\rm eff}$ of α Cen B. Their surface gravities and metallicities are also in line with our figures. Frutiger et al. (2005), inverting high-resolution line profiles, found a substantially lower [Fe/H], and their model-dependent $T_{\rm eff}$s agree either with our spectroscopic or with the photometric/Hα $T_{\rm eff}$, depending on assumptions. Their $\log g$ for α Cen B is also higher than all other recent determinations.

We discuss possible origins of the offset between the $T_{\rm eff}$ scales, concluding that the presence of NLTE effects, and also a possible inconsistency between spectroscopic and photometric $T_{\rm eff}$ scales, are probable explanations. Recent results reporting offsets between spectroscopic and photometric $T_{\rm eff}$ scales in cool stars, of similar magnitude, lend some credence to this interpretation. But we note that some authors claim consistency between the two scales, and that other sources of errors may be at play, such as uncertainties in the absolute flux calibration of photometric $T_{\rm eff}$s. We also note that recent claims of such $T_{\rm eff}$ offsets as caused by chromospheric activity cannot explain the present discrepancy given that both α Cen stars are considerably inactive stars. These discordant data still preclude a clear evaluation of the problem. For both α Cen A and B, the spectroscopic surface gravities agree well, within the uncertainties, with direct values derived from the dynamical masses of Pourbaix et al. (2002) and the radii of Kervella et al. (2003). The atmospheric parameters resulting from our analysis are collected in Table 3.

The abundance pattern of the system, when the various authors's data are considered for those elements for which at least three independent analyses are available, is found to be enriched in Na, Mg, Si, Mn, Co, Ni, and (with less reliability) Cu, and deficient in Y and Ba (Fig. 9). This abundance pattern is found to be in very good agreement with recent results on the abundance ratios of metal-rich stars. Thus, the system may be considered as a normal pair of middle-aged, metal-rich, thin disk stars.

An analysis of the evolutionary state of the system in the theoretical tracks of Kim et al. (2002) and Yi et al. (2003) yields a very good agreement of the evolutionary mass ($M_{\rm A} = 1.13 \pm 0.01$) and age (4.5–5.3 Gyr) of α Cen A with the results of recent seismological and dynamical data (Fig. 10). For α Cen B, a 1σ upward revision of its $T_{\rm eff}$ would bring its position in the HR diagram within reasonable agreement with the age found for α Cen A, and an evolutionary mass ($M_{\rm B} \sim 0.93$) in good agreement with the dynamical one would result. This merely marginal compatibility suggests that to fulfill the privileged situation of the α Cen system as a fundamental calibrator of the modelling of stellar structure and atmosphere models, additional analyses of component B seem to be necessary to quantify the onset and magnitude of possible NLTE in cool stars, as well as to allow for a more precise evaluation of possible offsets between spectroscopic and photometric $T_{\rm eff}$ scales in this class of objects.

Acknowledgements. We acknowledge fruitful discussions with Bengt Edvardsson. W.L. and G.R.K. wish to thank CNPq-Brazil for the award of a scholarship. G.F.P.M. acknowledges financial support by CNPq grant n° 476909/2006-6, FAPERJ grant n° APQ1/26/170.687/2004, and a CAPES post-doctoral fellowship n° BEX 4261/07-0. We thank the staff of the OPD/LNA for considerable support in the observing runs necessary for this project. Use was made of the Simbad database, operated at CDS, Strasbourg, France, and of NASA's Astrophysics Data System Bibliographic Services. We thank Dr. Monique Spite (Observatoire de Paris-Meudon) for use of the spectral line synthesis code. Criticism and suggestions from the anonymous referee have considerably improved the manuscript.

References

Abia, C., Rebolo, R., Beckman, J. E., & Crivellari, L. 1988, A&A, 206, 100
Allende-Prieto, C., Cobo, B. R., & García-López, R. J. 1998, ApJ, 502, 951
Allende Prieto, C., Barklem, P. S., Lambert, D. L., & Cunha, K. 2004, A&A, 420, 183 (ABLC04)
Anosova, J., Orlov, V. V., & Pavlova, N. A. 1994, A&A, 292, 115
Barklem, P. S., O'Mara, B. J., & Ross, J. E. 1998, A&A, 100
Bensby, T., Feltzing, S., & Lundström, I. 2003, A&A, 433, 185 (BFL03)
Bensby, T., Feltzing, S., Lundström, I., & Ylyin, I. 2005, A&A, 410, 527
Bessell, M. S. 1981, PASA, 4, 2
Bessell, M. S. 1990, A&AS, 83, 357
Bodaghee, A., Santos, N. C., Israelian, G., & Mayor, M. 2003, A&A, 404, 715 (BSIM03)
Böhm-Vitense, E. 1981, ARA&A, 19, 295
Casagrande, L., Portinari, L., & Flynn, C. 2006, MNRAS, 373, 13
Charbonnel, C., Däppen, W., Schaerer, D., Bernasconi, P. A., et al. 1999, A&AS, 135, 405
Chmielewski, Y., Friel, E., Cayrel de Strobel, G., & Bentolila, C. 1992, A&A, 263, 219
del Peloso, E. F., da Silva, L., & Porto de Mello, G. F. 2005a, A&A, 434, 275
del Peloso, E. F., Cunha, K., da Silva, L., & Porto de Mello, G. F. 2005b, A&A, 441, 1149
Doyle, M. T., O'Mara, B. J., Ross, J. E., & Bessell, M. S. 2005, PASA, 22, 6
Ecuvillon, A., Santos, N. C., Mayor, M., Villar, V., & Bihain, G. 2004, A&A, 426, 619
Edvardsson, B. 1988, A&A, 190, 148
Edvardsson, B., Andersen, J., Gustafsson, B., et al. 1993, A&A, 275, 101
Eggenberger, P., Charbonnel, C., Talon, S., et al. 2004, A&A, 417, 235
Endl, M., Kürster, M., Els, S., Hatzes, A. P., & Cochran, W. D. 2001, A&A, 374, 675
England, M. N. 1980, MNRAS, 191, 23
European Space Agency 1997, The Hipparcos Catalogue, Special Publication 120, ESA Publications Division, Nordwijk, The Netherlands
Flower, P. J. 1996, ApJ, 469, 355
French, V. A., & Powell, A. L. T. 1971, R. Obser. Bull., 173, 63
Frutiger, C., Solanki, S. K., & Mathys, G. 2005, A&A, 444, 549
Furenlid, I., & Meylan, T. 1990, ApJ, 350, 827 (FM90)
Girardi, L., Bressan, A., Bertelli, G., & Chiosi, C. 2000, A&AS, 141, 371
Gliese, W., & Jahreiss H. 1991, Preliminary Version of the Third Catalogue of Nearby Stars, Astronomisches Rechen-Institut, Heidelberg

Gratton, R. G., & Sneden, C. 1987, A&A, 178, 179
Gray, D. F., & Johanson, H. L. 1991, PASP, 103, 439
Gray, D. F., Tycner, C., & Brown, K. 2000, PASP, 112, 328
Grevesse, N., & Noels, A. 1993, in Origin and Evolution of the Elements, ed. N. Prantzos, E. Vangioni-Flam, & M. Cassé (Cambridge: Cambridge Univ. Press), 14
Guenther, D. B., & Demarque, P. 2000, ApJ, 531, 503
Gustafsson, B., Edvardsson, B., Eriksson, K., et al. 2008, A&A, 486, 951
Heiter, U., & Luck, R. E. 2003, AJ, 126, 2015
Holmberg, J., Flynn, C., & Portinari, L. 2006, MNRAS, 367, 449
Kervella, P., Thévenin, F., Ségransan, D., et al. 2003, A&A, 404, 1087
Kim, Y. C., Demarque, P., & Yi, S. K. 2002, ApJS, 143, 499
Kovtyukh, V. V., Soubiran, C., Belik, S. I., & Gorlova, N. I. 2003, A&A, 411, 559
Kurucz, R. L., Furenlid, I., Brault, J., & Testerman, L. 1984, Solar Flux Atlas from 296 to 1300 nm, National Solar Observatory
Lyra, W., & Porto de Mello, G. F. 2005, A&A, 431, 329
Lyra, W., Moitinho, A., van der Bliek, N., & Alves, J. 2006, A&A, 453, 101
Masana, E., Jordi, C., & Ribas, I. 2006, A&A, 450, 753
Meylan, T., Furenlid, I., Wigss, M. S., & Kurucz, R. L. 1993, ApJS, 85, 163
Miglio, A., & Montalbán, J. 2005, A&A, 441, 615
Moore, C. E., Minnaert, M. M., & Houtgast, J. 1996, The Solar Spectrum from 2935 Å to 8770 Å, Nat. Bur. Std., U.S. Monograph, 61
Morel, T., & Micela, G. 2004, A&A, 423, 677
Neuforge-Verheecke, C., & Magain, P. 1990, A&A, 328, 261
Porto de Mello, G. F., del Peloso, E. F. & Ghezzi, L. 2006, Astrobiology, 6, 308
Pourbaix, D., Neuforge-Verheecke, C., & Noels, A. 1999, A&A, 344, 172
Pourbaix, D., Nidever, D., McCarthy, C., et al. 2002, A&A, 386, 280
Ramírez, I., & Melendez, J. 2004, A&A, 609, 417
Ramírez, I., & Meléndez, J. 2005a, ApJ, 626, 446
Ramírez, I., & Meléndez, J. 2005b, ApJ, 626, 465
Ramírez, I., Allende-Prieto, C., & Lambert, D. L. 2007, A&A, 465, 271
Santos, N. C., Israelian, G., & Mayor, M. 2004, A&A, 415, 1153
Santos, N. C., Israelian, G., Mayor, M., et al. 2005, A&A, 437, 1127
Schaller, G., Schaerer, D., Meynet, G., & Maeder, A. 1992, A&AS, 96, 269
Schuler, S. C., King, J. R., Terndrup, D. M., et al. 2006a, ApJ, 636, 432
Schuler, S. C., Hatzes, A. P., King, J. R., Kürster, M., & The, L.-S. 2006b, AJ, 131, 1057
Shchukina, N., & Trujillo-Bueno, J. T. 2007, ApJ, 550, 970
Smith, G., Edvardsson, B., & Frisk, U. 1986, A&A, 165, 126
Soderblom, D. R. 1986, A&A, 158, 273
Spite, M. 1967, Ann. Astrophys., 30, 211
Steffen, M. 1985, A&AS, 59, 403
Thoul, A., Scuflaire, R., Noels, A., et al. 2003, A&A, 402, 293
Wertheimer, J. G., & Laughlin, G. 2006, AJ, 132, 1995
Valenti, J. A., & Fischer, D. A. 2005, ApJS, 159, 141
Yi, S. K., Kim, Y. C., & Demarque, P. 2003, ApJS, 144, 259
Yıldız, M. 2007, MNRAS, 374, 1264
Yong, D., Lambert, D. L., Allende Prieto, C., & Paulson, D. B. 2004, ApJ, 603, 697

Table 2. Spectral lines of the elements used in this study.

λ	χ	log gf	W_λ (mÅ)			λ	χ	log gf	W_λ (mÅ)			λ	χ	log gf	W_λ (mÅ)		
(Å)	(eV)		Moon	A	B	(Å)	(eV)		Moon	A	B	(Å)	(eV)		Moon	A	B
		Na I				5381.020	1.57	–1.855	65.9	79.0	80.9	5701.557	2.56	–2.116	89.2	99.5	127.9
6154.230	2.10	–1.532	40.6	62.5	92.3	5418.756	1.58	–2.116	52.8	66.9	55.8	5705.473	4.30	–1.427	42.1	53.0	66.8
6160.753	2.10	–1.224	60.5	86.3	120.4							5731.761	4.26	–1.115	60.9	71.1	85.9
								V I				5784.666	3.40	–2.487	33.0	42.8	61.0
		Mg I				5657.436	1.06	–0.889	8.5	10.4	40.4	5811.916	4.14	–2.383	11.3	17.6	26.3
5711.095	4.34	–1.658	112.2	124.3	...	5668.362	1.08	–0.940	7.3	11.7	38.2	5814.805	4.28	–1.851	23.7	33.6	44.7
5785.285	5.11	–1.826	59.0	68.3	88.7	5670.851	1.08	–0.396	21.6	31.4	82.1	5835.098	4.26	–2.085	16.2	22.8	35.0
						5727.661	1.05	–0.835	9.8	14.6	56.8	5849.681	3.69	–2.963	8.3	13.5	22.9
		Si I				6135.370	1.05	–0.674	14.1	20.6	59.6	5852.222	4.55	–1.180	43.2	54.3	71.3
5517.533	5.08	–2.454	14.5	25.5	21.8	6150.154	0.30	–1.478	12.9	20.4	65.5	5855.086	4.61	–1.521	24.5	34.8	42.8
5665.563	4.92	–1.957	43.0	57.0	62.3	6274.658	0.27	–1.570	11.1	15.0	60.6	5856.096	4.29	–1.553	36.6	48.1	61.2
5684.484	4.95	–1.581	65.1	79.4	78.6	6285.165	0.28	–1.543	11.5	25.1	66.3	5859.596	4.55	–0.579	77.4	88.4	105.6
5690.433	4.93	–1.627	63.2	67.4	64.6							6098.250	4.56	–1.760	17.7	25.7	35.4
5701.108	4.93	–1.967	41.9	57.3	58.2			Cr I				6120.249	0.92	–5.733	7.5	11.8	29.1
5708.405	4.95	–1.326	78.7	93.1	95.9	5214.144	3.37	–0.739	18.2	27.2	39.9	6137.002	2.20	–2.830	72.9	83.4	104.9
5793.080	4.93	–1.896	46.1	62.4	60.3	5238.964	2.71	–1.312	19.9	33.8	55.2	6151.616	2.18	–3.308	51.1	60.7	80.5
6125.021	5.61	–1.496	34.7	51.3	51.4	5272.007	3.45	–0.311	32.9	42.9	88.0	6173.340	2.22	–2.871	70.2	83.7	100.9
6142.494	5.62	–1.422	38.5	52.5	49.8	5287.183	3.44	–0.822	13.8	16.6	34.9	6219.287	2.20	–2.412	93.6	102.9	134.6
6145.020	5.61	–1.397	40.5	55.1	55.3	5296.691	0.98	–1.343	96.5	107.0	153.1	6226.730	3.88	–2.068	31.2	40.1	56.8
6243.823	5.61	–1.220	51.8	67.5	64.1	5300.751	0.98	–2.020	64.7	76.6	103.7	6240.645	2.22	–3.295	50.0	60.0	80.4
6244.476	5.61	–1.264	48.8	66.5	66.3	5304.183	3.46	–0.701	16.8	25.1	16.8	6265.131	2.18	–2.537	88.3	99.9	135.0
						5318.810	3.44	–0.647	19.2	27.9	53.4	6271.283	3.33	–2.703	26.5	36.7	54.9
		Ca I				5784.976	3.32	–0.360	34.0	48.0	72.9						
5261.708	2.52	–0.564	126.9	123.0	182.1	5787.965	3.32	–0.129	49.4	59.8	83.8			Fe II			
5867.572	2.93	–1.566	26.7	35.8	58.6							5234.630	3.22	–2.199	90.4	110.9	92.7
6161.295	2.52	–1.131	135.5	85.7	128.7			Cr II				5264.812	3.33	–2.930	53.1	67.2	64.8
6163.754	2.52	–1.079	126.6	87.7	93.8	5305.855	3.83	–2.042	27.1	37.8	24.1	5325.560	3.22	–3.082	51.1	66.3	52.7
6166.440	2.52	–1.116	72.6	88.9	114.0	5313.526	4.07	–1.539	38.7	49.3	43.4	5414.075	3.22	–3.485	33.7	46.0	32.1
6169.044	2.52	–0.718	97.7	113.4	158.0							5425.257	3.20	–3.229	45.5	58.1	46.3
6169.564	2.52	–0.448	118.5	137.5	185.8			Mn I				6149.249	3.89	–2.761	37.8	48.4	30.0
						5394.670	0.00	–2.916	83.4	103.8	165.0	6247.562	3.89	–2.325	57.1	69.6	48.3
		Sc I				5399.479	3.85	–0.045	42.9	63.4	96.6						
5671.826	1.45	0.538	16.1	24.2	64.1	5413.684	3.86	–0.343	28.0	45.8	73.1			Co I			
6239.408	0.00	–1.270	7.8	12.3	12.9	5420.350	2.14	–0.720	88.6	116.4	177.5	5212.691	3.51	–0.180	20.0	34.8	50.6
						5432.548	0.00	–3.540	54.9	73.3	141.0	5301.047	1.71	–1.864	22.5	33.8	57.9
		Sc II				5537.765	2.19	–1.748	37.3	57.4	113.3	5342.708	4.02	0.661	35.1	48.5	80.5
5318.346	1.36	–1.712	16.0	23.3	28.7							5359.192	4.15	0.147	11.9	20.1	37.3
5526.815	1.77	0.099	80.2	97.8	86.5			Fe I				5381.772	4.24	0.000	8.2	15.6	20.0
5657.874	1.51	–0.353	71.2	85.9	76.5	5054.647	3.64	–1.806	53.0	67.6	97.6	5454.572	4.07	0.319	18.9	26.8	42.8
5684.189	1.51	–0.984	40.4	55.6	48.9	5067.162	4.22	–0.709	85.4	90.3	123.1						
6245.660	1.51	–1.063	37.6	51.1	51.0	5109.649	4.30	–0.609	87.9	100.1	143.0			Ni I			
						5127.359	0.93	–3.186	109.6	117.7	164.8	5094.406	3.83	–1.088	32.4	45.0	62.2
		Ti I				5151.971	1.01	–3.128	108.9	120.8	177.5	5220.300	3.74	–1.263	28.5	40.6	52.1
5071.472	1.46	–0.683	36.1	45.7	99.0	5213.818	3.94	–2.752	7.5	13.0	20.2	5435.866	1.99	–2.340	57.4	73.8	88.9
5113.448	1.44	–0.815	30.9	36.4	98.3	5223.188	3.63	–2.244	32.3	41.6	56.5	5452.860	3.84	–1.420	19.0	29.1	37.3
5145.464	1.46	–0.615	39.6	50.8	90.6	5225.525	0.11	–4.577	83.2	92.7	128.8	5846.986	1.68	–3.380	24.2	35.8	56.9
5147.479	0.00	–1.973	43.7	66.8	102.7	5242.491	3.63	–1.083	92.3	107.5	132.2	6176.807	4.09	–0.315	61.2	86.8	90.1
5152.185	0.02	–2.130	34.9	43.5	79.1	5243.773	4.26	–0.947	69.6	84.3	91.5	6177.236	1.83	–3.476	16.4	29.4	41.2
5211.206	0.84	–2.063	9.3	13.7	...	5250.216	0.12	–4.668	78.1	96.1	136.0						
5219.700	0.02	–2.264	28.9	39.0	82.9	5321.109	4.43	–1.191	48.0	59.5	76.8			Cu I			
5295.780	1.07	–1.633	14.2	18.6	49.8	5332.908	1.56	–2.751	102.8	118.6	139.8	5218.209	3.82	0.293	55.9	71.8	82.5
5426.236	0.02	–2.903	9.0	12.1	48.2	5379.574	3.69	–1.542	64.8	76.5	94.4	5220.086	3.82	–0.630	15.5	25.0	32.5
5679.937	2.47	–0.535	8.6	10.1	28.8	5389.486	4.41	–0.533	87.3	102.2	123.0						
5866.452	1.07	–0.842	49.6	64.8	107.5	5395.222	4.44	–1.653	25.2	33.7	52.1			Y II			
6098.694	3.06	–0.095	6.9	10.1	27.6	5432.946	4.44	–0.682	76.4	90.2	106.7	5087.426	1.08	–0.329	49.3	53.7	54.2
6126.224	1.07	–1.358	25.3	31.9	68.3	5491.845	4.19	–2.209	14.3	25.4	32.9	5289.820	1.03	–1.847	4.5	5.6	7.7
6258.104	1.44	–0.410	54.2	65.5	102.5	5522.454	4.21	–1.418	46.8	59.9	70.4	5402.780	1.84	–0.510	14.7	22.2	22.1
						5560.207	4.43	–1.064	55.1	66.7	75.6						
		Ti II				5577.013	5.03	–1.415	14.5	20.3	26.3			Ba II			
5211.544	2.59	–1.551	33.5	46.1	35.2	5661.348	4.28	–1.802	25.5	33.6	48.6	5853.688	0.60	–0.828	67.5	73.4	68.6
5336.783	1.58	–1.592	76.7	90.0	89.7	5680.240	4.19	–2.255	13.2	19.1	27.8	6141.727	0.70	0.244	124.4	127.4	140.1